# Plasmon-Enhanced Quantum Dot Nanobeads-Based Lateral Flow Assay with Lower Background and Improved Sensitivity

*Xiaoyi Li1,2,3, Yucheng Wang3, Wannian Yan1, Yijie Tang4, Ru-jia Yu5, Huanxing Han6,*, Pengfei Zhang1,**

1 Department of Central Laboratory, Shanghai Skin Disease Hospital, School of Medicine, Tongji University, Shang-hai 200443, China.

2 Molecular Biology and Microbial Food Safety, Swammerdam Institute for Life Sciences, University of Amsterdam, Science Park 904, 1098 XH, Amsterdam, Netherlands.

3 Shanghai Kundao Biotech. Co., Ltd., Shanghai 201206, China.

4 Department of Laboratory Medicine, Shanghai Skin Disease Hospital, School of Medicine, Tongji University, Shanghai 200443, China.

5 State Key Laboratory of Analytical Chemistry for Life Science, School of Chemistry and Chemical Engineering, Nanjing University, Nanjing 210023, China.

6 Department of Pharmacy, Changzheng Hospital, Naval Medical University, Shanghai 200003, China.

KEYWORDS: point-of-care test, quantum dots nanobeads, plasmon-enhanced fluorescence, lateral flow assay, interleukin-6, gold nanoparticles

ABSTRACT

Developing a quantum dot (QD) nanobeads-based lateral-flow assay (LFA) is of great importance for achieving ultrasensitive, quantitative, and rapid testing of clinical specimens at the point-of-care. However, the QD nanobeads currently used in LFA still have drawbacks such as large particle size, which leads to high background, easy aggregation, and poor fluidity. To address these issues, a promising strategy is to utilize plasmonic energy transfer from gold nanoparticles (AuNPs) to QDs to create smaller size and brighter fluorescent QD nanobeads, without simply increasing the amount of QDs encapsulated in the nanobeads. In this study, we prepared the plasmon-enhanced quantum dot nano-beads (PEQNB) by encapsulating AuNPs and QDs into polymer nanobeads using the versatile emulsion-solvent evaporation method. We were able to detect as low as ~4347 PEQNBs nanoparticles using a gel imager, which is 14.6 times brighter than the QD nanobeads of a similar size. Compared to QD nanobeads of similar size, the PEQNB-based LFA for interleukin-6 detection exhibited higher fluorescent signal and lower background. The detection limit of PEQNB-based LFA was 1.63-fold higher than that of QD nanobeads. Furthermore, compared to larger-sized QD nanobeads with aver-age diameter of 131.1nm, PEQNB with average diameter of 78.6 nm based LFA exhibited similar levels of fluorescence intensity, but 1.55-fold lower background signal and 1.44-fold lower detection limits. This work demonstrates that optimized plasmon-enhanced QD nanobeads can further increase the sensitivity and lower the background signals of ultra-sensitive QD nanobeads-based LFA for disease diagnosis at point-of-care.

## Introduction

Recently, fluorescent lateral flow assays (LFA) using fluorescent nanoparticles as labels have been developed to improve sensitivity and precision of assay at point-of-care[1–3]. Fluorescent LFA strips employed various types of nanoparticles, including upconverting nanoparticles[4,5], time-resolved fluorescence nanoparticles[6–8], and quantum dots (QDs)[9–11]. The use of these nanoparticles as labels allows for quantitative measurements to be made by their fluorescence intensity on the LFA strips by a fluorescent reader. Notably, QDs exhibit unique optical properties suitable for use as labels in fluorescent LFA, including high brightness, resistance to photobleaching, excellent optical stability, tunable emission peaks, and ease of functionalization with bioreceptors[9,12–14]. Moreover, QDs-based LFA provides a more cost-effective and easier producibility solution alternative to time-resolved fluorescence nanoparticles based-LFA and upconverting nanoparticles due to their complicated preparation process and expensive testing equipment requirements[15].

Despite its advantages, QDs nanoparticles-based LFA is still limited in sensitivity and tedious antibody labeling procedures[16–18]. To address these limitations, quantum dots nanobeads (QNBs) are prepared using multiple nanoparticles encapsulated into the organic or inorganic nanobeads to provide signal amplification for fluorescent immunoassay, larger surface area for antigen-antibody binding, and increasing long-term stability by isolating QDs from the surrounding environment[19–21]. The preparation methods of QNBs include swelling method, layer-by-layer strategy and emulsion-solvent evaporation method[22–24]. For example, CdSe/ZnS quantum dots fluorescent nanospheres was prepared by the swelling method and showed that their luminescence capacity was 380 times higher than that of a single QD. The detection of C-reaction protein using LFA based on fluorescent nanospheres was 257 times more sensitive than conventional LFA based on AuNPs[25]. Magnetic microspheres with a triple QD shell (MagTQD) were prepared using a PEI-

mediated layer-by-layer self-assembly approach. A dual-mode LFA was then developed using MagTQD to detect SARS-CoV-2 spike (S) and nucleocapsid protein antigens, with ultrasensitive detection limits of 1 and 0.5 pg/mL for S and NP antigens in direct and enriched modes, respectively[11].

In our previous work, we prepared QNBs using a one-step process of emulsion-solvent evaporation technique. The results showed that QNBs were significantly more capable of coupling antibodies than QDs, and QNBs-based dot-blot immunoassay could detect hepatitis B surface antigen (HBsAg) protein down to 78 pg[26]. However, large nanobeads have some disadvantages, including high background signals, susceptibility to aggregation, and slow flow speed, which increase immunochromatography reaction time and decrease the dynamic range of assay[9,27–29]. Therefore, small-size fluorescent microspheres with a high loading of QDs are ideal for highly sensitive and quantitative LFA. Nevertheless, excessive loading of QDs into nanobeads result to increases the diameter of nanobeads, and partial fluorescence quenching due to the Förster resonance energy transferring between QDs.

It is well known that metal-based plasmonic nanostructures and nanoparticles can facilitate a variety of physicochemical reactions, including plasmon-enhanced fluorescence[30–32], enhanced photothermal and photocatalytic activity[33,34], and surface-enhanced Raman scattering (SERS)[35–37]. Although, the mechanism of plasmon-enhanced fluorescence is not fully understand, it is speculated to involve a combination process of enhanced local electromagnetic field, increased excitation rate of fluorophores, and decreased fluorescence lifetime.[31,38,39]. Many research groups have demonstrated that coupling fluorescent probes with plasmonic metal nanoparticles increases their fluorescence intensity. For example, Fu and his colleagues adsorbed single Cy3.5 dye molecules and mCherry fluorescent proteins on a 10 nm thick conformal surface over a gold

nanorod (NR) and observed up to 3.4-fold average enhancement of fluorescence intensity[40]. Plasmon-enhanced fluorescent nanocomposite consisting of a AuNP core, a thin PVP-coated layer, a silica spacer layer, and a fluorescent dye layer located in the silica matrix have also been reported[41–43]. Additionally, quantum dot-gold nanorod architecture with plasmon enhance fluorescence was reported with controlled spacing and quantum dot/nanorod ratio using organic or DNA molecule spacers[44–46]. However, the plasmon-enhanced fluorescent nanoparticles suffer from complicated preparation steps, and there is very limited research on quantum dots-gold nanoparticles composite-based LFA systems.

In this study, we proposed a plasmon-enhanced QNB (PEQNB) by doping a small amount of AuNPs into QNB. Rather than increasing the number of QDs to enhance the fluorescent intensity of QNB, PEQNB has smaller increase in the size of nanobeads. Using lateral flow assay for interlukin-6 (IL-6) detection as an example, PEQNB-based LFA is more sensitive than similar-size QNB-based LFA, due to higher fluorescent intensity of nanobeads. Moreover, the resulting smaller size of PEQNB exhibits reduced background signals compared to larger-sized QNB. This study introduces a straightforward approach to developing brighter and smaller labeling materials for LFA applications through a rational design strategy.

## Results and Discussion

### *Preparation of Plasmon-enhanced QD Nanobeads*

A simple, fast, and versatile emulsion-evaporation method was developed in our group to prepare various functional nanobeads, including QD nanobeads, AIE nanobeads and deeply dyed nanobeads. The plasmon-enhanced quantum dot nanobeads (PEQNB) was prepared by the emulsifying an oil phase solution containing QDs, AuNPs and amphiphilic polymer in a water phase with SDS surfactant, followed by evaporation of oil solvent (chloroform), as shown in

Figure 1a. AuNPs of size ~8.2 nm (Figure S1a) and CdSe/ZnS quantum dots of size ~11.8 nm were simultaneously encapsulated into polymer nanobeads with a diameter of ~100 nm.

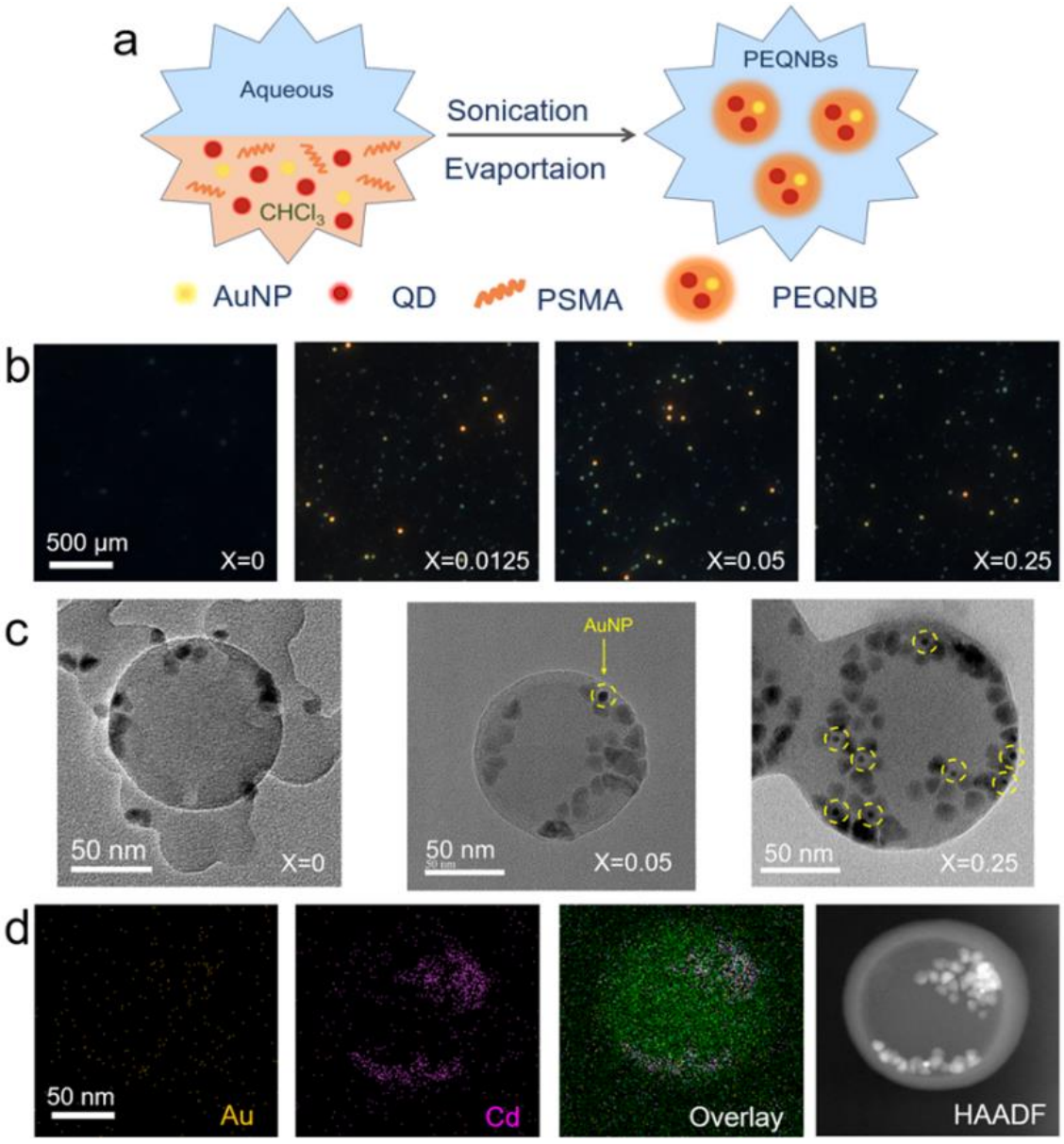


**Figure 1.** (a) Schematic illustration of the preparation process of the plasmon-enhanced quantum dots nanobeads (PEQNB) using the emulsion-solvent evaporation method. (b) Dark-field microscopy images of nanobeads with Au/QD weight ratio (X) of 0, 0.0125, 0.05 and 0.25. (c) TEM images of nanobeads with Au/QDs ratio (X) of 0, 0.05 and 0.25, and the AuNPs marked with

yellow circular. (d) Element mapping results of Au, PEQNB and HAADF-STEM image of PEQNB (X = 0.05).

The plasmon-enhanced fluorescence is attributed to plasmon coupling facilitated by a non-radiative interaction[47,48]. A key point to note is that the ratio and distance of AuNPs and QDs strongly influences the plasmon-enhanced fluorescent effect. Different weight ratios of AuNPs/QDs indirectly cause changes in the distance between QDs and AuNPs, leading to a continuous transition from fluorescence enhancement to quenching[30]. Therefore, we maintained a constant concentration of QDs and adjusted the amount of AuNPs to obtain the optimal enhancement effect. We carried out dark-field scattering measurements, and the corresponding microscopic images not only confirmed that AuNPs were successfully assembled in nanobeads, but also demonstrated the plasmon function of AuNPs (Figure 1b). The morphologies of nanobeads with Au/QD weight ratio of 0, 0.05 and 0.25 were investigated using the transmission electron microscopy (TEM), as shown in Figure 1c. The TEM images indicated that AuNPs and QDs were assembled into spherical nanobeads (diameter of ~100 nm) with different Au/QDs ratio. The AuNPs were obviously observed in the nanobead with smaller size and higher electron density, and were marked with yellow circular rings in Figure 1c. The structure of a single PEQNB was investigated by high-angle annular dark-field scanning transmission electron microscopy (HAADF-STEM), where AuNPs were observed inside a spherical matrix (Figure 1d). Energy-dispersive X-ray spectroscopy (EDS) mapping of PEQNB demonstrated a distribution of cadmium based QDs nanoparticles in the nanobead, with Au nanoparticles dispersed sporadically.

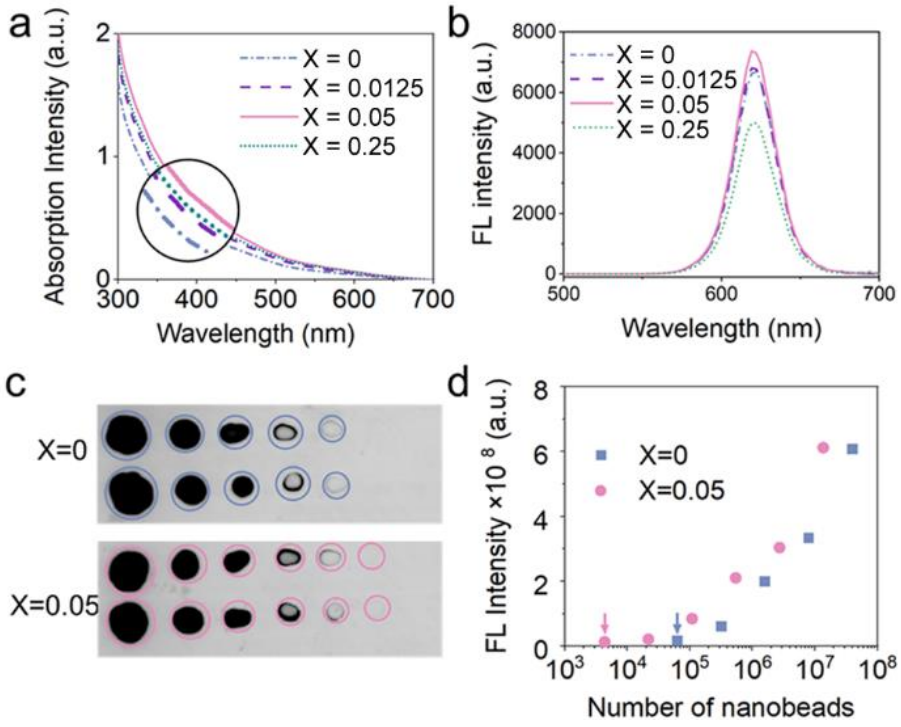


**Figure 2.** UV–vis absorption (a) and fluorescence (FL) (b) spectra of nanobeads with Au/QD weight ratio (X) of 0, 0.0125, 0.05 and 0.25. (c) fluorescence dot images obtained from PVDF membrane drop-casted with the same particles concentrations of QDs nanobeads without Au (X = 0) and with Au (X = 0.05). (d) Corresponding fluorescence intensity obtained dot images.

***Plasmon-enhanced fluorescence of PEQNB***

To investigate the AuNPs doping ratio with optimized plasmon-enhanced fluorescence effect, absorption and fluorescence (FL) spectra were measured. Figure 2a showed the normalized absorption intensity of QNB without AuNPs and with Au/QD weight ratio (X) of 0.0125, 0.05 and 0.25. As the amount of AuNPs increased, the absorption intensity of the QNBs suspension with the same particle concentration initially rose, and then decreased. Notably, at X= 0.25, it decreases lower than QNB, which may attribute to aggregation of AuNPs with themselves or with QDs at high concentration. The highest absorption intensity was exhibited when X= 0.05. The

fluorescence (FL) spectra of nanobeads were measured with excitation light of 365 nm, and the obtained spectra are shown in Figure 2b, with the nanobeads emitting peak at around 619 nm. Like the pattern of absorption intensity, the PL intensity increased and then decreased with increasing AuNPs weight ratio. The highest FL intensity of PEQNB ensemble was observed at Au ratio of X= 0.05.

In addition, we compared the fluorescence intensity of PEQNB with QNB by a dot-blot assay on the polyvinylidene difluoride (PVDF) membrane. We dropped a known amount of serially diluted QNB and PEQNB onto a PVDF membrane to determine the minimum numbers of QNB and PEQNB required to produce detectable fluorescent signals. It required an accumulation of 63530 QNBs to produce a detectable signal, but only 4347 PEQNB were needed (Figure 2d). The dot-blot assay results indicated that PEQNB had a 14.6-fold lower concentration threshold than QNB for a detectable fluorescence signal. Additionally, the fluorescent intensity of single nanobead was investigated by imaging analysis of over 100 nanobeads on the fluorescent micrographs, as shown in Figure S2. The average fluorescent intensity of single PEQNB was about 2.2 times higher than single QNB.

***Comparison of QNB and PEQNB-based LFA***

We utilized a sandwich immunoassay to detect interlukin-6 (IL-6) to verify the enhanced performance of PEQNB as labels for lateral flow assay. Human IL-6 capture antibodies and DNP-BSA hapten were immobilized on a nitrocellulose (NC) membrane to form a test line and control line, respectively, as shown in Figure 3a. QNB and PEQNB were covalently functionalized with IL-6 detection antibodies to obtain QNB@IL-6 and PEQNB@IL-6 fluorescent antibody conjugates, employing carbodiimide chemistry for carboxyl groups activation. QNB functionalized with anti-DNP were used as a detector ligand (QNB@anti-DNP) for the control

line. According to the signal-noise ratio (SNR) from LFA test, the optimized conjugation ratio of PEQNB and antibodies was 1 mg nanobeads and 100 μg antibody, as depicted in Figure S3.

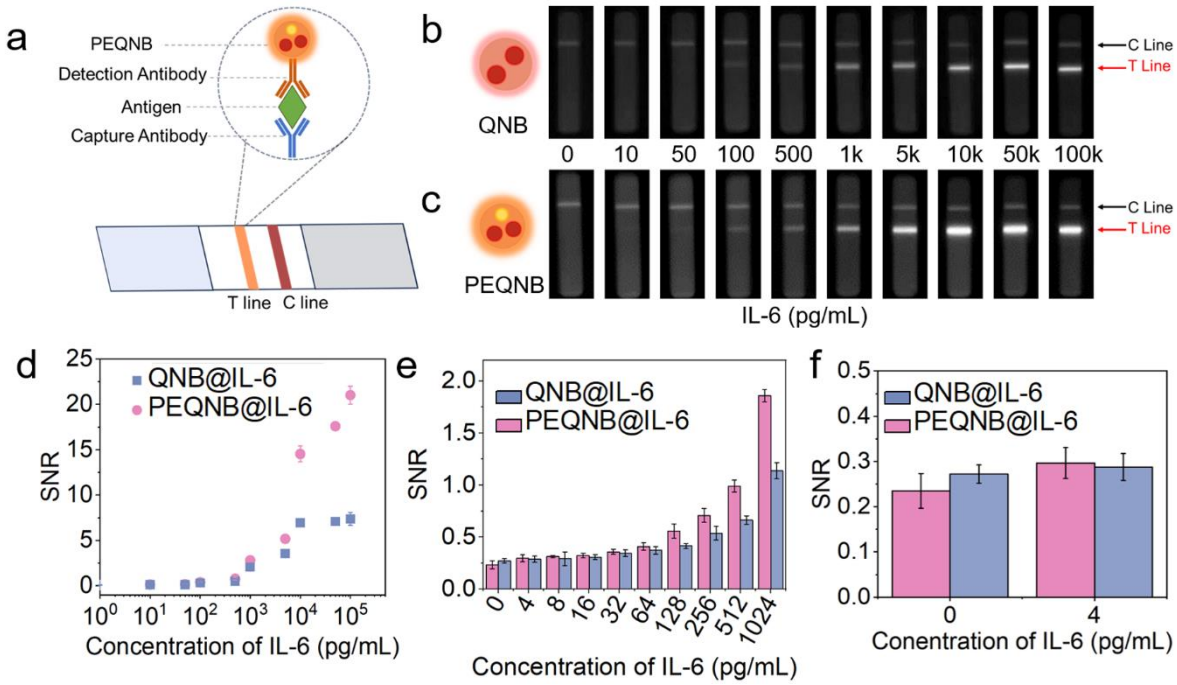


**Figure 3**. (a) Schematic illustration of the IL-6 LFA strips comprising IL-6 capture antibody as test line and DNP-BSA hapten as control line. Fluorescence images of the IL-6 LFA strips reaction with QNB@IL-6 (b) and PEQNB@IL-6 (c), and all fluorescence images were split into grayscale images of red channel by Image J. (d) Dose-dependent signal-noise ratio (SNR) corresponding to different concentrations of IL-6 acquired from the same particle concentration of PEQNB and QNB based LFA (n=3). Analytical SNR performance (e) and background signals (f) of fluorescence LFA based on the same mass concentration of PEQNB and QNB (n=6).

A series of IL-6 calibrator solutions were prepared by diluting recombinant IL-6 proteins with dilution buffer, and then mixed with nanobead-antibody conjugates solution. The mixture was added into the sample hole of LFA and allowed to react for 15min to ensure optimal SNR response, as shown in Figure S4. Accumulation of a sufficient number of nanobeads, the test line was able

to be read in red color under a UV lamp, indicating a positive result and the presence of the target analyte, as shown in Figure S7. The greyscale intensity of fluorescence signals at the test line of LFA based on QNB and PEQNB increased with the concentration of the IL-6 (Figure 3b, c). Remarkably, when the same particles concentration of QNB and PEQNB were loaded, the QNB-based LFA under the UV lamp was visible at 100 pg/mL IL-6 (Figure 3b). However, PEQNB produced a naked-eye readable fluorescent signal at 50 pg/mL (Figure 3c). Furthermore, we used a fluorescence strip reader to quantify the fluorescence signal from these LFA strips. The results showed that the quantitative fluorescence signal of PEQNB was approximately twice as high as same particle concentration of QNB at high concentration of IL-6 (Figure 3d). The limit of detection (LOD) (defined as mean + 3σ of the blank; σ is the standard deviation) of QNB-based LFA is calculated to be 21.3 pg/mL (Figure S5b), while the LOD of PEQNB-based LFA is 13.1 pg/mL (Figure S5a). Similarly, the LOQ (defined as mean + 10σ of the blank) of QNB-based LFA is 65.8 pg/mL, and the LOQ of PEQNB-based LFA is 36.4 pg/mL.

Moreover, the same wight concentration of QNB@IL-6 and PEQNB@IL-6 fluorescent conjugates were added for the LFA, where the number of nanobeads in the QNB fluorescence solution was ~2.9 times the number of nanobeads in PEQNB (Figure 3e). Following a similar procedure to the previous assay, the quantitative results of QNB and PEQNB-based LFA were shown in Figure 3e and 3f. PEQNB-based LFA has a lower background signal than QNB-based LFA for negative sample (Figure 3f). At the rest of the calibrator points, PEQNB-based LFA has a higher signal-to-noise (SNR) ratio. Especially at concentration of 1024 pg/mL, the SNR ratio of PEQNB-based LFA is 1.6 times higher than QNB-based LFA. Overall, the results above indicated that PEQNB-base LFA demonstrated improved sensitivity, enhanced fluorescence signal response and lower background signals, compared with similar-size QNB-based LFA.

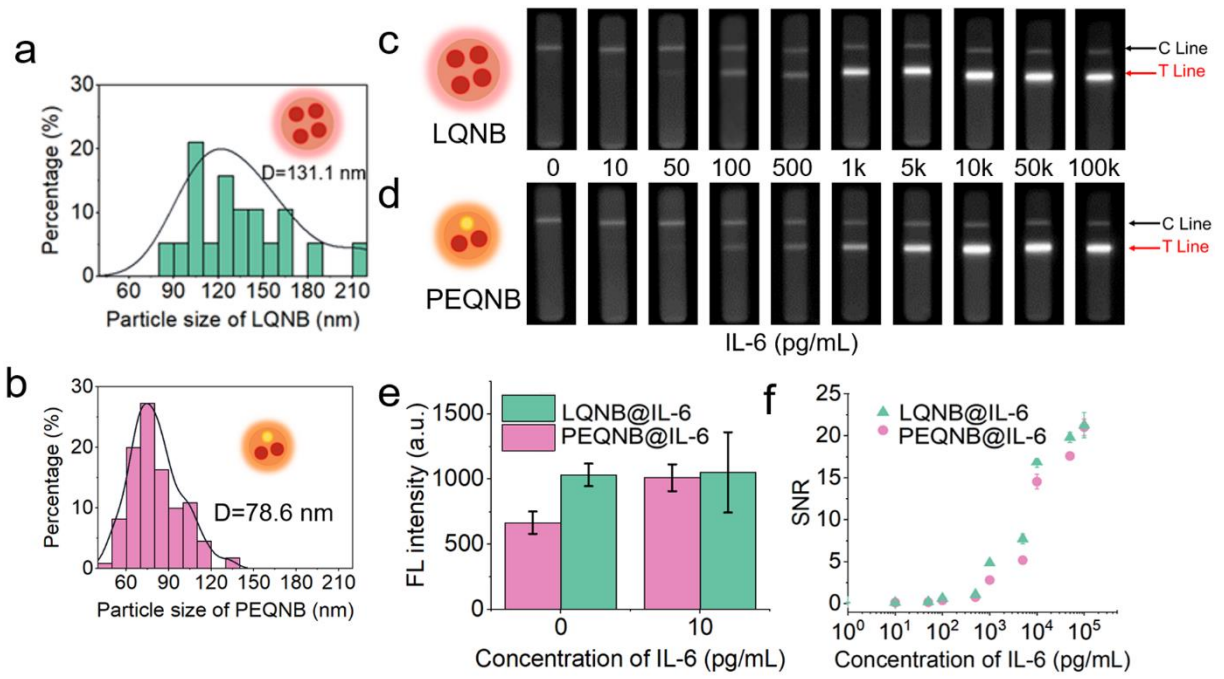


**Figure 4.** Size distribution of (a) LQNB with average diameter of 131.1 nm and (b) PEQNB with average diameter of 78.6 nm were measured from TEM image analysis. Fluorescence images of the IL-6 LFA strips reaction with LQNB@IL-6 (c) and PEQNB@IL-6 (d), all the fluorescence images were split into grayscale images of R channel by Image J. (e) Compared to LQNB, PEQNB-based LFA has lower background fluorescent signal when IL-6 concentration is 0 pg/mL (negative sample) and similar fluorescent signal when IL-6 is 10 pg/mL (weak positive sample). (f) Dose-dependent SNR corresponding to different concentrations of IL-6 acquired from PEQNB and LQNB-based LFA (n=3).

### *Comparison of PEQNB and LQNB-based LFA*

Generally, increasing the size of nanobeads resulted more QDs being encapsulated in nanobeads and enhancing the fluorescent intensity of nanobeads. However, larger size of nanobeads lead to decreased fluidity of nanobeads on NC membrane and higher background signals. To study the size effect, the performance of PEQNB-based LFA was compared with that of larger-sized

quantum nanobeads (LQNB). The sizes of nanobeads were measured from the TEM images, as shown in Figure S1. The histograms of the particle size distributions for the LQNB and PEQNB nanobeads are presented in Figure 4a and 4b. The histograms were fitted to the Kernel-Smooth distribution function, and the peak values were taken as average particle size that is 131.1 nm and 78.6 nm.

As shown in Figure 4c and 4d, the fluorescence signals of LQNB-based LFA and PEQNB-based LFA both increased with the concentration of IL-6, and were visible at a minimum of 50 pg/mL under UV light illumination. When comparing the blank and weak negative (10 pg/mL) data, the results demonstrated that the LQNB-based LFA exhibited a higher background fluorescence compared to the PEQNB-based LFA (Figure 4e), which may be attributed to the reduction in diffusivity and subsequent particle retention in the NC membrane. For quantitative analysis, the testing results of PEQNB and LQNB showed similar patterns, as shown in Figure 4f. The LOD and LOQ of PEQNB-based LFA were calculated to be 13.1 and 36.4 pg/mL, and the LOD and LOQ of LQNB-based LFA were 18.8 pg/mL and 46.9 pg/mL, as shown in Figure S5. The coupling between the resonance frequency of the AuNPs and the frequency of the QD emission may lead to elastic scattering, resulting in an increase in the excitation efficiency of the quantum dots and fluorescence of the entire nanobead[30,49]. The PEQNB has similar fluorescent intensity to LQNB composed of more QDs and larger volume. Therefore, the PEQNB-based LFA enables low background signal and ultrasensitive detection of target analyte over a broader range of analyte concentration.

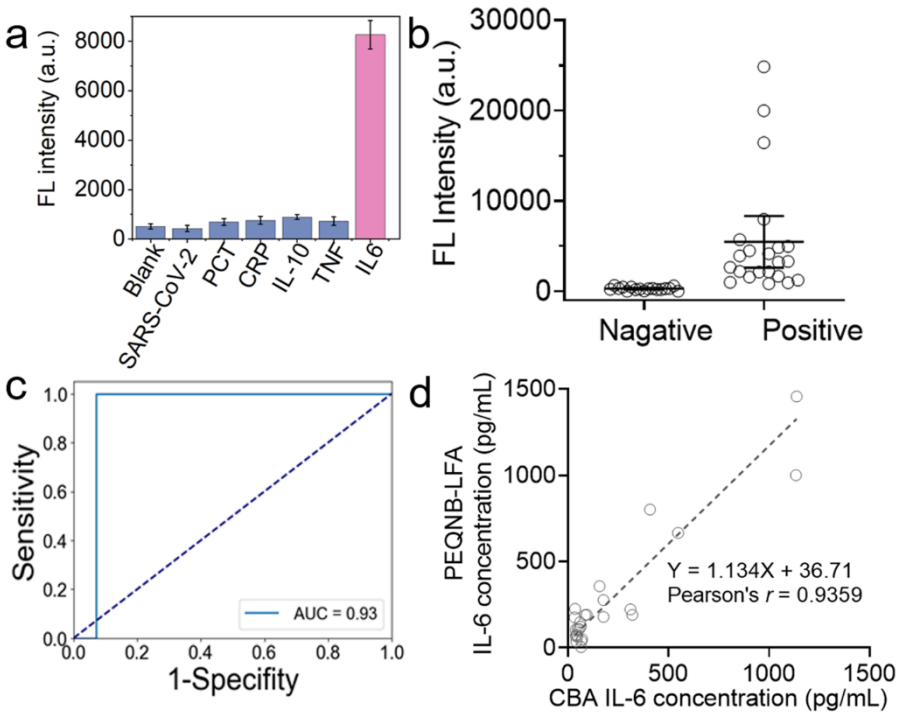


**Figure 5.** (a) Evaluation of the specificity of the PEQNB@IL-6-based LFA system. (b) Fluorescence intensity of PEQNB@IL-6-based LFA in patient samples (17 control samples and 22 positive samples). (c) Receiver operating characteristic (ROC) curves and area under the curves (AUC) of the PEQNB@IL-6-based LFA system. (d) Correlation analysis between of the PEQNB-based LFA system and the cytometric bead array (CBA) method for IL-6 detection.

***Specificity and clinical validation***

The specificity of PEQNB@IL-6 LFA was investigated using several other inflammatory biomarkers, including procalcitonin (PCT), C-reactive protein (CRP), interleukin 10 (IL-10), tumor necrosis factor (TNF), and coronavirus nucleocapsid protein (SARS-CoV-2 NP). Spike-in samples containing the interference proteins (1000 pg/mL) were prepared and measured using our proposed PEQNB-based LFA. In addition, IL-6 sample (1000 pg/mL) and blank sample were used as positive and negative controls, respectively. As shown in Figure 5a, the fluorescence signals from spike-in samples and negative control were relatively low, while the IL-6 positive sample

exhibited a significant fluorescence intensity. These results indicated that PEQNB-based LFA can specifically distinguish IL-6 from other common inflammatory biomarkers and coronaviruses.

The clinical reliability of the PEQNB-based LFA was further evaluated by conducting assays of IL-6 in 33 clinical serum samples, including 16 positive samples from clinical patients and 17 negative samples (<2.5 pg/mL). As shown in Figure 5b, the fluorescent intensities of test line in positive samples are significantly higher than those in clinical negative samples. The receiver operating characteristic (ROC) curve, with an area under the curve (AUC) of 0.93, indicated that PEQNB-base LFA was sensitive and specific for IL-6 detection in clinical samples, with a cut-off value of 20 pg/mL. The testing results were also compared with those obtained from cytometric bead array (CBA) method. Figure 5d demonstrated a strong correlation between the PEQNB-based LFA and the clinical CBA method, with Pearson's correlation coefficient ($r$) of 0.9359. The results obtained from the clinical samples testing indicated that the developed PEQNB-based LFA was well corelated with CBA method for the specific and rapid detection of IL-6 in human serum samples.

**Conclusion**

In conclusion, we have successfully prepared plasmon-enhanced QD nanobeads with adjustable Au/QDs weight ratios using a versatile emulsion-solvent evaporation method. The ensemble fluorescent intensity of the optimized PEQNB, with Au/QD weight ratio of 0.05, is 14.6-fold brighter than QNB containing the same amount of QDs and polymer. PEQNB-based LFA for IL-6 detection is 1.63 times more sensitive than similar-size QNB-based LFA, and is as sensitive as larger-size QNB-based LFA. Furthermore, compared to QNB, PEQNB with optimized Au/QD ratio is brighter than QNB of the same size, owing to the localized surface plasmon resonance of AuNPs around them. This smaller size and brighter PEQNB-based LFA demonstrated lower

background signals than the larger-size QNB, and exhibited a higher fluorescent response at high-dose samples. However, the plasmonic resonance of metal nanoparticles is highly depending on the size and shape of metal nanoparticles, which warrants further investigation to achieve optimized PEQNB. Additionally, the size of nanobeads plays a critical role in the sensitivity of LFA and should also be studied. All in all, this facile PEQNB fabrication method may serve as a new strategy to enhance the sensitivity of QD nanobeads and other fluorescent nanobeads-based LFA.

**Experimental Section**

**Synthesis of QNB and PEQNB.** A typical procedure for the synthesis of QNB or PEQNB is based on the emulsion-solvent evaporation method. Plasmon-enhanced quantum dots nanobeads were composed of amphiphilic co-polymer, gold nanoparticles (AuNPs) and CdSe/ZnS core/shell quantum dots. Typically, the oil-soluble AuNPs nanoparticles (8.2 nm, 1mg/mL), CdSe/ZnS quantum dots (~15 nm, 20 mg/mL) and PSMA (30 mg/mL) were dispersed together in 5 mL of chloroform to obtain the oil phase solution. The oil phase and 0.1% SDS aqueous solution were mixed in a volume ratio of 1:3 and stirred magnetically (300 rpm) at room temperature for 0.5 hours. The miniemulsion was obtained by ultrasonication for 1 min (3 s pulse, 3 s pause) at 25% amplitude with a sonicator (Fisher Sonic Dismembrator Model 500, USA). The miniemulsion was magnetically stirred for 24 hours in an open container at room temperature and then centrifuged (13,000 rpm, 10 min). The plasmon-enhanced fluorescent nanobeads were obtained by the washed pellet with deionized water.

**Preparation of nanobeads-antibody conjugates.** Antibodies conjugates of nanobeads (QNB or PEQNB) were prepared by the conventional EDC coupling reaction between the amino groups of the antibodies and carboxyl groups on the hydrophilic surface of nanobeads. Briefly, 100 μL of

nanobeads (10 mg/mL) solution was dispersed in 200 μL of phosphate buffer (0.02 M, pH 6.0), followed by activation with 6 μL (20 mg/mL) EDC. The activated nanobeads were gently shaken for 30 min at room temperature and then centrifuged at 15,000 rpm for 10 min. After removing the supernatant, the activated solution was resuspended in 100 μL of phosphate buffer and ultrasound for 5 min. IL-6 detection antibody (100 μg) was dispersed in 200 μL of phosphate buffer, then it was rapidly added to the activated nanobeads solution, the mixture was incubated for 30 min at room temperature and then centrifuged at 8000 rpm for 5 min. The terminated pellet was incubation 2 hours by using 200 μL of blocking solution (BSA 1%) at room temperature and then stored in 100 μL of storing buffer (BSA 1%, sucrose 5%, PVP 1%, S9 0.2%, and TO-7 0.2%) at 4°C. To functionalize nanobeads with antibodies (anti-DNP), a similar process was used.

**Preparation of LFA test strips.** LFA strips consist of sample pad, nitrocellulose (NC) membrane, absorbent pad and polystyrene adhesive backing card. IL-6 capture antibody and DNP-BSA hapten were respectively diluted to the concentration of 1 mg/mL and 0.8 mg/mL in phosphate buffer (0.02 M, pH 6.0) and then sprayed onto the NC membrane (1 μL/cm) as a test and control line by a dispensing platform (HAS 520, Hangzhou Fenghang, China). They were placed in a desiccator at 20 °C and 7 % humidity for 24 h. After drying, the sample pads, NC membranes and absorbent pads were assembled onto the polyvinyl chloride adhesive backing card with an overlap of 1-2 mm between each part. The well-assembled master plates are cut into 3.8 mm wide strips using a strip cutter (Hangzhou Fenghang, China). Each strip is packed into a strip housing cassette with a circular sample loading hole and rectangular viewing window for further use.

**Detection of IL-6 with LFA.** The antigen dilution buffer was prepared by PBS buffer, with 20% trehalose dihydrate, 5% BSA, and 0.2% proclin-300. A series of IL-6 calibrators with

concentrations ranging from 0 to 10000 pg/mL were prepared by using the dilution buffer. The immunoassay fluorescent conjugates solution was prepared by diluting PEQNB@IL-6 conjugate with storing buffer (PBS, with 1% BSA, 10% trehalose, 0.5% PEG, 0.5 PVP, 0.2% S9, and 0.2% TO-7). Typically, 50 μL fluorescent conjugate solution with 50 μL calibrator or sample was mixed and then added to the sample pad of LFA strips. Each sample was measured repeat three times and the fluorescence signals were collected after 15 min. The photos of LFA strips were recorded by a phone camera under UV light illumination. Color photos were split into grayscale images of red, green, and blue channels using the Image J software (NIH, USA), and red channel images were used for analysis. The fluorescence signals were quantitatively measured by using a fluorescent LFA reader (FIC-Q100, Suzhou Hemai, China).

**Specificity and human serum samples measurement.** The specificity of PEQNB@IL-6 LFA was evaluated as follows. Interference proteins including IL-6, procalcitonin (PCT), C-reactive protein (CRP), interleukin 10 (IL-10), tumor necrosis factor-α (TNF-α), and SARS-CoV-2 NPs with concentrations of 1000 pg/mL were prepared by using the antigen dilution buffer. The 50 μL fluorescent conjugates solution buffer was mixed with the interference samples (50 μL) and then placed on the sample pad of an IL-6 LFA strip.

Human serum samples were collected from Shanghai Skin Disease Hospital, with ethical permission (2021-28). The standard level of the IL-6 concentration was tested by Cytometric Bead Array (CBA) method. The serum calibrators were prepared by diluting of positive serum sample (1137.17 pg/mL) with negative serum sample (less than 2.5pg/mL) to obtain the calibrated curves for serum samples measurement. All of the human serum samples (50 μL) were added into 50 μL of running buffer, and the mixture was added onto the sample pad of an IL-6 LFA strip. As the fluid moved from the sample pad to the absorbent pad, the fluorescent IL-6 conjugates and DNP

conjugates were captured at the test line and control line, respectively. The corresponding fluorescence intensities were measured after 15 min.

**Supporting Information.**

The Supporting Information is available free of charge online.

Materials; Synthesis of AuNPs; Characterization; TEM images of AuNPs, PEQNB, and LQNB; Fluorescent micrographs; Conjugation reaction optimization; Effect of reaction time; Fitting curves of LFAs; Fluorescence images of LFAs. (PDF)

AUTHOR INFORMATION

**Corresponding Authors**

**Pengfei Zhang** - Department of Central Laboratory, Shanghai Skin Disease Hospital, School of Medicine, Tongji University, Shanghai 200443, China.

Email: pfzhang@tongji.edu.cn

**Huanxing Han** - Department of Pharmacy, Changzheng Hospi-tal, Naval Medical University, Shanghai 200003, China.

Email: huanxing_han@163.com

**Authors**

**Xiaoyi Li** - Department of Central Laboratory, Shanghai Skin Disease Hospital, School of Medicine, Tongji University, Shanghai 200443, China; Molecular Biology and Microbial Food Safety, Swammerdam Institute for Life Sciences, University of Amsterdam, Science Park 904,

1098 XH, Amsterdam, Netherlands; Shanghai Kundao Biotech. Co., Ltd., Shanghai 201206, China.

**Yucheng Wang** - Shanghai Kundao Biotech. Co., Ltd., Shanghai 201206, China.

**Wannian Yan** - Department of Central Laboratory, Shanghai Skin Disease Hospital, School of Medicine, Tongji University, Shanghai 200443, China.

**Yijie Tang** - Department of Laboratory Medicine, Shanghai Skin Disease Hospital, School of Medicine, Tongji University, Shanghai 200443, China.

**Ru-Jia Yu** - State Key Laboratory of Analytical Chemistry for Life Science, School of Chemistry and Chemical Engineering, Nanjing University, Nanjing 210023, China.

**Funding Sources**

This work was supported by the Project of Shanghai Science and Technology Committee (STCSM) (20S31902800, 22S31902000), and Clinical Research Incubation Program of Shanghai Skin Disease Hospital (NO. lcfy2021-10).

**Notes**

The authors declare no competing financial interest.

ACKNOWLEDGMENT

The authors thank prof. Yi-Tao Long for extremely helpful comments and discussions.

REFERENCES

(1) Ao, L.; Liao, T.; Huang, L.; Lin, S.; Xu, K.; Ma, J.; Qiu, S.; Wang, X.; Zhang, Q. Sensitive and Simultaneous Detection of Multi-Index Lung Cancer Biomarkers by an NIR-II Fluorescence Lateral-Flow Immunoassay Platform. *Chem. Eng. J.* **2022**, *436*, 135204. https://doi.org/10.1016/j.cej.2022.135204.

(2) Miller, B. S.; Bezinge, L.; Gliddon, H. D.; Huang, D.; Dold, G.; Gray, E. R.; Heaney, J.; Dobson, P. J.; Nastouli, E.; Morton, J. J. L.; McKendry, R. A. Spin-Enhanced Nanodiamond Biosensing for Ultrasensitive Diagnostics. *Nature* **2020**, *587* (7835), 588–593. https://doi.org/10.1038/s41586-020-2917-1.

(3) Boehringer, H. R.; O'farrell, B. J. Lateral Flow Assays in Infectious Disease Diagnosis. *Clin. Chem.* **2022**, *68* (1), 52–58. https://doi.org/10.1093/clinchem/hvab194.

(4) Ji, T.; Xu, X.; Wang, X.; Zhou, Q.; Ding, W.; Chen, B.; Guo, X.; Hao, Y.; Chen, G. Point of Care Upconversion Nanoparticles-Based Lateral Flow Assay Quantifying Myoglobin in Clinical Human Blood Samples. *Sensors Actuators B Chem.* **2019**, *282*, 309–316. https://doi.org/10.1016/j.snb.2018.11.074.

(5) Huang, Z.; Liu, Y.; Chen, Y.; Xiong, Q.; Wang, Y.; Duan, H.; Lai, W. Improving the Performance of Upconversion Nanoprobe-Based Lateral Flow Immunoassays by Supramolecular Self-Assembly Core/Shell Strategies. *Sensors Actuators, B Chem.* **2020**, *318* (February), 128233. https://doi.org/10.1016/j.snb.2020.128233.

(6) Ye, Z.; Tan, M.; Wang, G.; Yuan, J. Novel Fluorescent Europium Chelate-Doped Silica Nanoparticles: Preparation, Characterization and Time-Resolved Fluorometric Application. *J. Mater. Chem.* **2004**, *14* (5), 851. https://doi.org/10.1039/b311905j.

(7) Xia, X.; Xu, Y.; Ke, R.; Zhang, H.; Zou, M.; Yang, W.; Li, Q. A Highly Sensitive Europium Nanoparticle-Based Lateral Flow Immunoassay for Detection of Chloramphenicol Residue. *Anal. Bioanal. Chem.* **2013**, *405* (23), 7541–7544. https://doi.org/10.1007/s00216-013-7210-9.

(8) Hu, L.; Luo, K.; Xia, J.; Xu, G.; Wu, C.; Han, J. Biosensors and Bioelectronics Advantages of Time-Resolved Fl Uorescent Nanobeads Compared with Fl Uorescent Submicrospheres , Quantum Dots , and Colloidal Gold as Label in Lateral Fl Ow Assays for Detection of Ractopamine. *Biosens. Bioelectron.* **2017**, *91* (December 2016), 95–103. https://doi.org/10.1016/j.bios.2016.12.030.

(9) Fang, B.; Xiong, Q.; Duan, H.; Xiong, Y.; Lai, W. Tailored Quantum Dots for Enhancing Sensing Performance of Lateral Flow Immunoassay. *TrAC Trends Anal. Chem.* **2022**, *157*, 116754. https://doi.org/10.1016/j.trac.2022.116754.

(10) Jia, J.; Ao, L.; Luo, Y.; Liao, T.; Huang, L.; Zhuo, D.; Jiang, C.; Wang, J.; Hu, J. Quantum Dots Assembly Enhanced and Dual-Antigen Sandwich Structured Lateral Flow Immunoassay of SARS-CoV-2 Antibody with Simultaneously High Sensitivity and Specificity. *Biosens. Bioelectron.* **2022**, *198* (November 2021), 113810. https://doi.org/10.1016/j.bios.2021.113810.

(11) Wang, C.; Cheng, X.; Liu, L.; Zhang, X.; Yang, X.; Zheng, S.; Rong, Z.; Wang, S. Ultrasensitive and Simultaneous Detection of Two Specific SARS-CoV-2 Antigens in Human Specimens Using Direct/Enrichment Dual-Mode Fluorescence Lateral Flow Immunoassay. *ACS Appl. Mater. Interfaces* **2021**, *13* (34), 40342–40353. https://doi.org/10.1021/acsami.1c11461.

(12) Huang, B.; Yang, H.; Zhang, L.; Yuan, Y.; Cui, Y.; Zhang, J. Effect of Surface/Interfacial Defects on Photo-Stability of Thick-Shell CdZnSeS/ZnS Quantum Dots. *Nanoscale* **2018**, *10* (38), 18331–18340. https://doi.org/10.1039/C8NR04224A.

(13) Ren, M.; Xu, H.; Huang, X.; Kuang, M.; Xiong, Y.; Xu, H.; Xu, Y.; Chen, H.; Wang, A. Immunochromatographic Assay for Ultrasensitive Detection of Aflatoxin $B_1$ in Maize by Highly Luminescent Quantum Dot Beads. *ACS Appl. Mater. Interfaces* **2014**, *6* (16), 14215–14222. https://doi.org/10.1021/am503517s.

(14) Michalet, X.; Pinaud, F. F.; Bentolila, L. A.; Tsay, J. M.; Doose, S.; Li, J. J.; Sundaresan, G.; Wu, A. M.; Gambhir, S. S.; Weiss, S. Quantum Dots for Live Cells, in Vivo Imaging, and Diagnostics. *Science.* **2005**, *307* (5709), 538–544.

(15) Guo, J.; Chen, S.; Guo, J.; Ma, X. Nanomaterial Labels in Lateral Flow Immunoassays for Point-of-Care-Testing. *J. Mater. Sci. Technol.* **2021**, *60*, 90–104. https://doi.org/10.1016/j.jmst.2020.06.003.

(16) Bailes, J. Photostability of Semiconductor Quantum Dots in Response to UV Exposure. *Nanoparticles Biol. Med. Methods Protoc.* **2020**, 343–349.

(17) Arnspang Christensen, E.; Kulatunga, P.; Lagerholm, B. C. A Single Molecule Investigation of the Photostability of Quantum Dots. *PLoS One* **2012**, *7* (8), e44355.

(18) Zrazhevskiy, P.; Gao, X. Quantum Dot Imaging Platform for Single-Cell Molecular Profiling. *Nat. Commun.* **2013**, *4*, 1612–1619. https://doi.org/10.1038/ncomms2635.

(19) Banerjee, A.; Pons, T.; Lequeux, N.; Dubertret, B. Quantum Dots–DNA Bioconjugates: Synthesis to Applications. *Interface Focus* **2016**, *6* (6), 20160064. https://doi.org/10.1098/rsfs.2016.0064.

(20) Malekzad, H.; Hasanzadeh, M.; Shadjou, N.; Jouyban, A. Highly Sensitive Immunosensing of Prostate Specific Antigen Using Poly Cysteine Caped by Graphene Quantum Dots and Gold Nanoparticle: A Novel Signal Amplification Strategy. *Int. J. Biol. Macromol.* **2017**, *105*, 522–532. https://doi.org/10.1016/j.ijbiomac.2017.07.069.

(21) Yang, Y.; Liu, Q.; Liu, Y.; Cui, J.; Liu, H.; Wang, P.; Li, Y.; Chen, L.; Zhao, Z.; Dong, Y. A Novel Label-Free Electrochemical Immunosensor Based on Functionalized Nitrogen-Doped Graphene Quantum Dots for Carcinoembryonic Antigen Detection. *Biosens. Bioelectron.* **2017**, *90*, 31–38. https://doi.org/10.1016/j.bios.2016.11.029.

(22) Mattoussi, H.; Palui, G.; Na, H. Bin. Luminescent Quantum Dots as Platforms for Probing in Vitro and in Vivo Biological Processes. *Adv. Drug Deliv. Rev.* **2012**, *64* (2), 138–166.

(23) Nakata, Y.; Mukai, K.; Sugawara, M.; Ohtsubo, K.; Ishikawa, H.; Yokoyama, N. Molecular Beam Epitaxial Growth of InAs Self-Assembled Quantum Dots with Light-Emission at 1.3 Mm. *J. Cryst. Growth* **2000**, *208* (1–4), 93–99.

(24) Valizadeh, A.; Mikaeili, H.; Samiei, M.; Farkhani, S. M.; Zarghami, N.; kouhi, M.; Akbarzadeh, A.; Davaran, S. Quantum Dots: Synthesis, Bioapplications, and Toxicity. *Nanoscale Res. Lett.* **2012**, *7* (1), 480. https://doi.org/10.1186/1556-276X-7-480.

(25) Hu, J.; Zhang, Z.-L.; Wen, C.-Y.; Tang, M.; Wu, L.-L.; Liu, C.; Zhu, L.; Pang, D.-W. Sensitive and Quantitative Detection of C-Reaction Protein Based on Immunofluorescent Nanospheres Coupled with Lateral Flow Test Strip. *Anal. Chem.* **2016**, *88* (12), 6577–6584. https://doi.org/10.1021/acs.analchem.6b01427.

(26) Zhang, P.; Lu, H.; Chen, J.; Han, H.; Ma, W. Simple and Sensitive Detection of HBsAg by Using a Quantum Dots Nanobeads Based Dot-Blot Immunoassay. *Theranostics* **2014**, *4* (3), 307–315. https://doi.org/10.7150/thno.8007.

(27) Duan, H.; Chen, X.; Wu, Y.; Leng, Y.; Huang, X.; Xiong, Y. Integrated Nanoparticle Size with Membrane Porosity for Improved Analytical Performance in Sandwich Immunochromatographic Assay. *Anal. Chim. Acta* **2021**, *1141*, 136–143. https://doi.org/10.1016/j.aca.2020.10.041.

(28) Khlebtsov, B. N.; Tumskiy, R. S.; Burov, A. M.; Pylaev, T. E.; Khlebtsov, N. G. Quantifying the Numbers of Gold Nanoparticles in the Test Zone of Lateral Flow Immunoassay Strips. *ACS Appl. Nano Mater.* **2019**, *2* (8), 5020–5028. https://doi.org/10.1021/acsanm.9b00956.

(29) Zhan, L.; Guo, S. Z.; Song, F.; Gong, Y.; Xu, F.; Boulware, D. R.; McAlpine, M. C.; Chan, W. C. W.; Bischof, J. C. The Role of Nanoparticle Design in Determining Analytical Performance of Lateral Flow Immunoassays. *Nano Lett.* **2017**, *17* (12), 7207–7212. https://doi.org/10.1021/acs.nanolett.7b02302.

(30) Li, J.-F.; Li, C.-Y.; Aroca, R. F. Plasmon-Enhanced Fluorescence Spectroscopy. *Chem. Soc. Rev.* **2017**, *46* (13), 3962–3979. https://doi.org/10.1039/C7CS00169J.

(31) Fothergill, S. M.; Joyce, C.; Xie, F. Metal Enhanced Fluorescence Biosensing: From Ultra-Violet towards Second near-Infrared Window. *Nanoscale* **2018**, *10* (45), 20914–20929. https://doi.org/10.1039/c8nr06156d.

(32) Cui, Y.; Yuan, C.; Tan, H.; Zhang, Z.; Jia, Y.; Na, N.; Ouyang, J. Plasmon-Enhanced Fluorescent Sensor Based on Aggregation-Induced Emission for the Study of Protein Conformational Transformation. *Adv. Funct. Mater.* **2019**, *29* (10). https://doi.org/10.1002/adfm.201807211.

(33) Shi, R.; Cao, Y.; Bao, Y.; Zhao, Y.; Waterhouse, G. I. N.; Fang, Z.; Wu, L. Z.; Tung, C. H.; Yin, Y.; Zhang, T. Self-Assembled Au/CdSe Nanocrystal Clusters for Plasmon-Mediated Photocatalytic Hydrogen Evolution. *Adv. Mater.* **2017**, *29* (27), 1–7. https://doi.org/10.1002/adma.201700803.

(34) Yin, H.; Yi, J.; Yang, Z. W.; Xu, Z. Y.; Xie, S. J.; Li, L.; Li, C. Y.; Xu, J.; Zhang, H.; Zhang, S. J.; Li, J. F.; Tian, Z. Q. Plasmon Enhanced Quantum Dots Fluorescence and Energy Conversion in Water Splitting Using Shell-Isolated Nanoparticles. *Nano Energy* **2017**, *42* (April), 232–240. https://doi.org/10.1016/j.nanoen.2017.10.055.

(35) Reiner, A. T.; Fossati, S.; Dostalek, J. Biosensor Platform for Parallel Surface Plasmon-Enhanced Epifluorescence and Surface Plasmon Resonance Detection. *Sensors Actuators B Chem.* **2018**, *257*, 594–601.

(36) Kumar, A.; Kim, S.; Nam, J.-M. Plasmonically Engineered Nanoprobes for Biomedical Applications. *J. Am. Chem. Soc.* **2016**, *138* (44), 14509–14525.

(37) Tan, L.-L.; Wei, M.; Shang, L.; Yang, Y.-W. Cucurbiturils-Mediated Noble Metal Nanoparticles for Applications in Sensing, SERS, Theranostics, and Catalysis. *Adv. Funct. Mater.* **2021**, *31* (1), 2007277. https://doi.org/10.1002/adfm.202007277.

(38) Jeong, Y.; Kook, Y.-M.; Lee, K.; Koh, W.-G. Metal Enhanced Fluorescence (MEF) for Biosensors: General Approaches and a Review of Recent Developments. *Biosens. Bioelectron.* **2018**, *111*, 102–116. https://doi.org/10.1016/j.bios.2018.04.007.

(39) Taylor, A. B.; Zijlstra, P. Single-Molecule Plasmon Sensing: Current Status and Future Prospects. *ACS Sensors* **2017**, *2* (8), 1103–1122. https://doi.org/10.1021/acssensors.7b00382.

(40) Fu, B.; Flynn, J. D.; Isaacoff, B. P.; Rowland, D. J.; Biteen, J. S. Super-Resolving the Distance-Dependent Plasmon-Enhanced Fluorescence of Single Dye and Fluorescent Protein Molecules. *J. Phys. Chem. C* **2015**, *119* (33), 19350–19358. https://doi.org/10.1021/acs.jpcc.5b05154.

(41) Chen, J.; Jin, Y.; Fahruddin, N.; Zhao, J. X. Development of Gold Nanoparticle-Enhanced Fluorescent Nanocomposites. *Langmuir* **2013**, *29* (5), 1584–1591. https://doi.org/10.1021/la3036049.

(42) Gupta, R.; Gupta, P.; Wang, S.; Melnykov, A.; Jiang, Q.; Seth, A.; Wang, Z.; Morrissey, J. J.; George, I.; Gandra, S.; Sinha, P.; Storch, G. A.; Parikh, B. A.; Genin, G. M.; Singamaneni, S. Ultrasensitive Lateral-Flow Assays via Plasmonically Active Antibody-Conjugated Fluorescent Nanoparticles. *Nat. Biomed. Eng.* **2023**. https://doi.org/10.1038/s41551-022-01001-1.

(43) Hong, D.; Jo, E. J.; Bang, D.; Jung, C.; Lee, Y. E.; Noh, Y. S.; Shin, M. G.; Kim, M. G. Plasmonic Approach to Fluorescence Enhancement of Mesoporous Silica-Coated Gold Nanorods for Highly Sensitive Influenza A Virus Detection Using Lateral Flow

Immunosensor. *ACS Nano* **2023**, *17* (17), 16607–16619. https://doi.org/10.1021/acsnano.3c02651.

(44) Draz, M. S.; Fang, B. A.; Li, L.; Chen, Z.; Wang, Y.; Xu, Y.; Yang, J.; Killeen, K.; Chen, F. F. Hybrid Nanocluster Plasmonic Resonator for Immunological Detection of Hepatitis B Virus. *ACS Nano* **2012**, *6* (9), 7634–7643. https://doi.org/10.1021/nn3034056.

(45) Li, J. Y.; Li, W.; Liu, J.; Zhong, J.; Liu, R.; Chen, H.; Wang, X. H. Room-Temperature Strong Coupling Between a Single Quantum Dot and a Single Plasmonic Nanoparticle. *Nano Lett.* **2022**, *22* (12), 4686–4693. https://doi.org/10.1021/acs.nanolett.2c00606.

(46) Chen, H.; Tian, F.; Lu, C. Engineering Plasmon-Enhanced Fluorescent Gold Nanoclusters Using Bovine Serum Albumin as a Novel Separation Layer for Improved Selectivity. *Anal. Chem.* **2022**, *94* (47), 16461–16469. https://doi.org/10.1021/acs.analchem.2c03925.

(47) Aslan, K.; Leonenko, Z.; Lakowicz, J. R.; Geddes, C. D. Annealed Silver-Island Films for Applications in Metal-Enhanced Fluorescence: Interpretation in Terms of Radiating Plasmons. *J. Fluoresc.* **2005**, *15*, 643–654.

(48) Lakowicz, J. R.; Ray, K.; Chowdhury, M.; Szmacinski, H.; Fu, Y.; Zhang, J.; Nowaczyk, K. Plasmon-Controlled Fluorescence: A New Paradigm in Fluorescence Spectroscopy. *Analyst* **2008**, *133* (10), 1308–1346.

(49) Geddes, C. D.; Lakowicz, J. R. Metal-Enhanced Fluorescence. *J. Fluoresc.* **2002**, *12*, 121–129.